Effects of Pr^{3+}-activated $BaZrGe_3O_9$@TiO_2 phosphor compound on light emitting diodes validated by computer simulation

Le Thi Trang[1], Le Xuan Thuy[2], Nguyen Le Thai[3], Thuc Minh Bui[4]
[1]Faculty of Information Technology, Dong Nai Technology University, Bien Hoa City, Vietnam
[2]Faculty of Basic Sciences, Vinh Long University of Technology Education, Vinh Long Province, Vietnam
[3]Faculty of Engineering and Technology, Nguyen Tat Thanh University, Ho Chi Minh City, Vietnam
[4]Faculty of Electrical and Electronics Engineering, Nha Trang University, Nha Trang City, Vietnam

Article Info

ABSTRACT

The Pr^{3+}-doped $BaZrGe_3O_9$ gallogermanate phosphors are reported to have a well-defined successive deep defect structure that effectively mitigates thermal carrier fading. This phosphor also presents a red emission with a peak at 615 nm, originating from the Pr^{3+} transtition from $^1D_2$ to $^3H_4$. We investigated the impact of Pr^{3+}-activated $BaZrGe_3O_9$ (referred to as BZG:Pr) on the lighting characteristics of light emitting diodes (LED) packages in this paper. By combining BZG:Pr with TiO_2 particles and silicone, we produced a phosphor layer (designated as BZG:Pr@TiO_2). The optical performance of the resulting LED was systematically examined by varying the TiO_2 doping percentage. Our findings reveal that the incorporation of the BZG:Pr phosphor enhances the red spectral component, thereby contributing to improved homogeneity in color distribution. However, a progressive increase in TiO_2 content within the phosphor layer corresponds to diminishing luminous output and decreased chromatic rendering efficiency of the LED. Employing a lower concentration of TiO_2 proves advantageous, as it capitalizes on the scattering-enhancing attributes while leveraging the red emission of the BZG:Pr phosphor. This synergistic approach yields a favorable balance between luminosity and color quality, enhancing the LED's overall performance.

Corresponding Author:

Thuc Minh Bui
Faculty of Electrical and Electronics Engineering, Nha Trang University
Nha Trang City, Vietnam
Email: minhbt@ntu.edu.vn

1. INTRODUCTION

Light emitting diodes, commonly known as LEDs, have revolutionized the world of lighting and display technology [1], [2]. These compact and energy-efficient devices have found their way into a multitude of applications, ranging from household lighting and electronics to medical equipment and automotive lighting. Moreover, high-energy LEDs have been applied to construct optical sensing or imaging instruments by utilizing the ultraviolet or near-infrared radiation to excite the luminescent materials [3]-[5]. However, one of the problems when utilizing the phosphor luminescent materials is that their luminescence performance is often degraded in high-thermal environments [6]. Besides, the commercial LED, using blue-pumped LED and yellow phosphor, is reported to have low color production accuracy as the generated white light does not include the red-light components [7]-[9]. Thus, it is critical to find a novel red phosphor material that can provides red emission under high-energy excitation source is critical. The red-emission photo-stimulated luminescent phosphors could be a potential candidate to overcome the mentioned problem.

Particularly, when such phosphors are subjected to elevated-energy radiation sources (X-ray or ultraviolet), the trapping centers capture the charge carriers. These captured carriers are subsequently liberated, through optical stimulation, towards emitting centers, culminating in emissions within the visible or near-infrared spectrum [10]. They also possess remarkable characteristics including heightened imaging sensitivity, cost-effectiveness of imaging equipment, and their compatibility with image-guided surgical procedures [11]. Yet, under long high-temperature operation, the phosphor struggles from the accerlated release of trapped carriers caused by the thermo-disturbance issue, reducing the phosphor efficiency in sensing or imaging application. The use of good thermostability host lattice can be a solution to improve this situation.

Among various phosphor host, the gallogermanate phosphors has drawn many interests owing to their luminescent properties. They are composed of zinc, gallium, germanium, and oxygen, and can be doped with various ions to produce different colors of light. Some of the applications of gallogermanate phosphors include white LEDs, bioimaging, and security labels. The $BaZrGe_3O_9$ (BZG) in the gallogermanate group possesses low-temperature synthesis and excellent stability, making it a promising novel phosphor base for both divalent and trivalent lanthanide dopants [12]. Besdies, Pr^{3+} ions when used as an activator introduce a compelling opportunity for the concurrent generation of blue, green, and red emissions within the context of laser action [13]. Therefore, the inclusion of Pr^{3+} in the BZG can establish a consecutive defect arrangement within the host matrix. This Pr^{3+}-activated BZG phosphor gave out the red emission centering at 615 nm with the 980-nm simulation wavelength owing to the Pr^{3+} transition from $^1D_2$ to $^3H_4$. It also shown deep traps of 0.85-0.98 eV, contributing to mitigating the thermal fading of charge carriers, leading to enhancement in the temperature-resistance ability [14]. We took the Pr^{3+}-activated $BaZrGe_3O_9$ (BZG:Pr) to examine its effects on the lighting properties of LED package. The BZG:Pr is mixed with TiO_2 particles and silicone to make a phosphor layer (BZG:Pr@TiO_2). The illuminating characteristics of the prepared LED is determined with TiO_2 doping percentage variation. Results show the presence of BZG:Pr phosphor results in the enhancement of red spectrum to obtain the better color distribution homogeneity. However, the increasing amount of the TiO_2 in the phosphor layer lead to the decreasing luminous power and chromatic reproducing efficiency of the LED. Low level of TiO_2 can help obtain good luminosity and color quality by accomplishing scattering improvement while utilizing the red-emission of BZG:Pr phosphor.

2.   METHOD

We prepared the BZG:Pr phosphor via the traditional solid-phase high-temperature reaction route [15], [16]. The initial materials employed encompassed high-purity (≥99%) $BaCO_3$, ZrO_2, GeO_2, and Pr_6O_{11}. The concentration of Pr^{3+} in the compound was determined at 0.0075. These precursor materials with stoichiometric proportion were mixed by grinding in an agate mortar, supplemented with appropriate quantities of ethanol, for a duration of 20 minutes. Following this blending step, the sample underwent sintering at 1,200 °C for a period of 3.5 hours, employing a heating rate of approximately 6 °C per minute under an ambient air atmosphere. After the sintering procedure, the samples were gradually cooled to room temperature within the furnace and subsequently re-ground for further investigations. The luminescence of the phosphor was measured with the Hitachi F-7000 fluorescence spectrophotometer. The white LED used for optical tests was structured with a cluster of InGaN chips (402 nm), a phosphor structure comprised of three phosphor types, including Sm-SGSS red phosphor, $BaMgAl_{10}O_{17}$:Eu^{2+} blue phosphor, and $(Ba,Sr)_2SiO_4$:Eu^{2+} green phosphor. The LED driving current was set at 20 mA and 3 V input. The lighting performances of constructed WLED were recorded and examined with different concentration values of the Sm-SGSS red phosphor. The LED fabrication illustration was shown in Figure 1. In Figures 1(a) and 1(b), the actual WLED created via conformal phosphor coating approach is presented. Elements of the WLED dual-layer design within the study herein are demonstrated via specifications. The reflector was designed at 2.07 m (height), 8 mm (bottom span) and 9.85 mm (top span); YAG:Ce^{3+} layer (0.08 mm thickness) would be put on LED dies. The 9 LED chips are linked with the gap in the reflectors, see Figures 1(c) and 1(d). Each of them exhibits 1.16 W radiant flux and 453 nm apex wavelength as well as having the size of 1.14 mm^2×0.15 mm (square base x altitude).
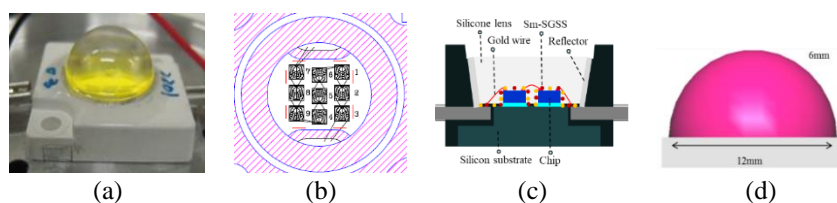
Figure 1. Photograph of WLEDs structure: (a) actual WLEDs, (b) bonding diagram, (c) illustration of pc-WLEDs model, and (d) simulation of WLEDs using LightTools commercial software

3. RESULTS AND DISCUSSION

In the investigation of how BZG:Pr@TiO$_2$ compound influence the prepared LED package, the concentration of TiO$_2$ particles is adjusted while the BZG:Pr amount is contant. In the way, it is possible to regulate the scattering factor for higher incident light utilization and conversion by the BZG:Pr phosphor. Figure 2 shows the scattering factor of the package with different values of TiO$_2$ weight percentage in the phosphor compound. The scattering coefficients in Figure 2 enhances with the increase in TiO$_2$ amounts, regardless of monitored wavelengths. This accomplished the initial objective in promoting the scattering performance of light within the package. The scattering performance under each light wavelength shows noticeable differences. The most remarkable scattering coefficients is observed in the case of 780 nm while the lowest is under 580 nm wavelength. The scattering value collected under the 380 nm wavelength is in the second place. These findings illuminate the utilization of BZG:Pr@TiO$_2$ compound in the development of near-infrared (780 nm) or ultraviolet (380 nm) illumination devices [17], [18].

Upon examination of BZG:Pr emissions at 615 nm, the exitation spectrum of the phosphor exhibit a broad band with three peaks at 300 nm, 449 nm, and 480 nm. The origins of the 300 nm centered bands are attributed to the 4f-5d transitions within the Pr^{3+} ions and the host material's absorption. Correspondingly, the presence of the two 449 nm and 480 nm peaks can be correlated to the Pr^{3+} transitions from $^3H_4$ to $^3P_2$ and $^3P_0$ [19]. This indicates that the BZG:Pr can be also used as a red-luminesence phosphor for the LED with blue chip. The emission power of the LED package with blue chip and a thin layer of yellow phosphor (YAG:Ce) in presence of phosphor compound BZG:Pr@TiO$_2$ is displayed in Figure 3. Note that the concentration of YAG:Ce phosphor must be lowered on the rising amount of TiO$_2$ in the compound as shown in Figure 4. This inversion between two material concentrations is to maintain the stability of correlated color temperature (CCT). The lower concentration of YAG:Ce phosphor also contribute to promoting the blue-light absorption and conversion by the BZG:Pr phosphors.

The emergence of distinct sharp peaks within the orange-red spectrum, noted in Figure 3, becomes pronounced as the TiO$_2$ concentration increases. When the TiO$_2$ particles are initially introduce to the phosphor compound with the amount of 10 wt%, the spectrum shows two prominent peaks around ~465 nm and ~594 nm, with the latter exhibiting considerably higher intensity than the former, as shown in Figure 3(a). This observation aligns with the characteristic luminescence of the BZG:Pr red phosphor. However, as the TiO$_2$ content is progressively augmented, the intensity of the blue peak diminishes gradually while multiple emission peaks in the wavelength range of 550-650 nm appears more obviously, as displayed in Figures 3(b) and 3(c). When the concentration of TiO$_2$ is at 40-50 wt%, it easy to see in the graphs three eminent emission peaks of 550 nm, 590 nm, and 615 nm [20]-[23], see Figure 3(d) and Figure 3(e). These results can be attributed to the scattering enhancement inducing the blue-light utilization of the yellow-green and red phosphor materials. However, the emission spectrum in Figure 3 exhibits decreasing intensity with the progressive augmentation of TiO$_2$ concentration. This phenomenon can be attributed to the redundant light scattering, culminating in an associated energy dissipation. Consequently, the increased energy loss contributes to a decline in the overall lumen output of the LED package, as clearly demonstrated in Figure 5. The lumen output demonstrates a gradual and considerable decline as the TiO$_2$ doping level escalates to 50 wt%, as a result of the attenuated blue emission peak and the decreased peak intensity within the yellow-red regions.
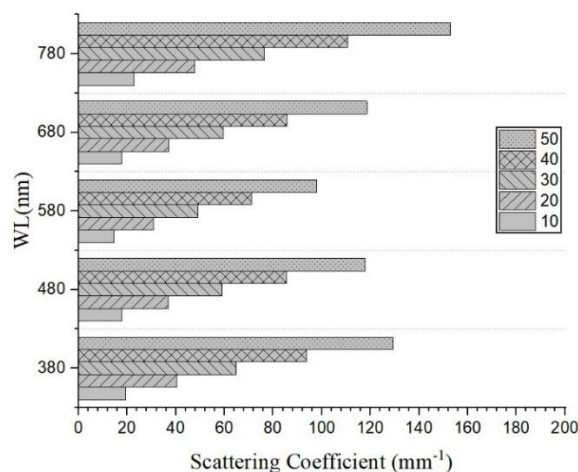
Figure 2. Scattering coefficients of the BZG:Pr@TiO$_2$ layer when varying TiO$_2$ amount

(a)

(b)

(c)

(d)

(e)
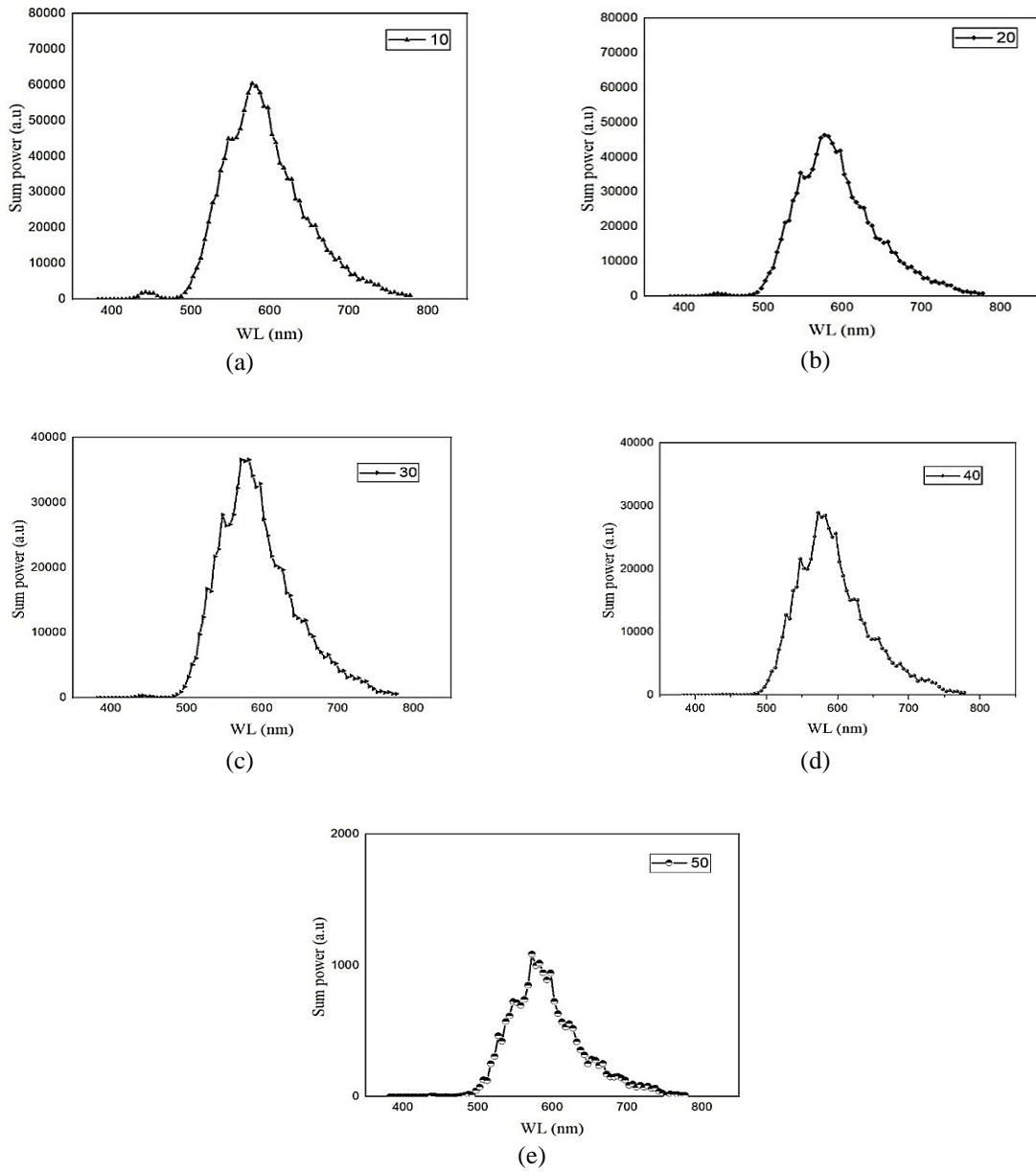
Figure 3. The emission spectrum when varying TiO_2 amount in BZG:Pr@TiO_2 compound: (a) 10%, (b) 20%, (c) 30%, (d) 40%, and (e) 50%
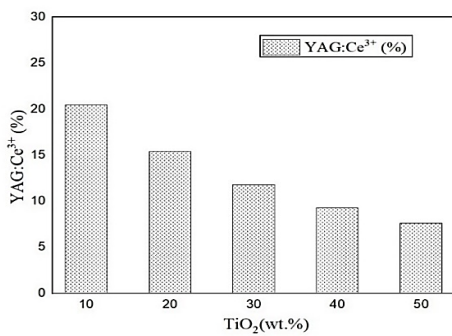
Figure 4. YAG:Ce concentration when varying TiO_2 amount in BZG:Pr@TiO_2 compound
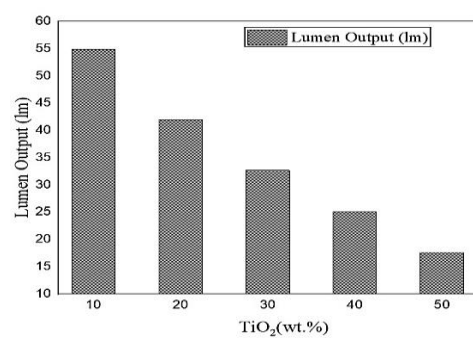
Figure 5. The lumen output when varying TiO_2 amount in BZG:Pr@TiO_2 compound

The assessment of the color reproducing capabilities of white LEDs employing the BZG:Pr@TiO$_2$ layer involves an evaluation of chromatic distribution uniformity and rendition performance. In the context of the former, we examined the angular CCT range and calculated the deviation in CCT levels, as depicted in Figure 6. In Figure 6(a), the presence of BZG:Pr@TiO$_2$ compound with TiO$_2$ mount from 10-40 wt%, the CCT range fluctuates but with an insignificant amount. However, with BZG:Pr@50wt% TiO$_2$, the difference between the highest and lowest CCT levels become larger. This can be vadilated using the calculated delta-CCT values in Figure 6(b). Delta CCT, calculated as the difference between maximum and minimum CCT values, serves as a metric for color uniformity, with a lower value indicating higher uniformity. Notably, the highest delta-CCT is recorded with 50 wt% TiO$_2$ concentration. The lowest delta-CCT is accomplished when TiO$_2$ is about 20 wt%. The delta-CCT with 10 wt% and 40 wt% TiO$_2$ is equal and much lower than that with 50 wt% of TiO$_2$. In other words, the integration of TiO$_2$ with the amount lower than 50wt% can bring uniform color distribution or higher color uniformity [24]-[26].

The color quality scale (CQS) and the color rendering index (CRI), illustrated in Figures 7 and 8, are utilized for the color rendering assessments. The CQS, a comprehensive parameter developed by researchers at the National Institute of Standards and Technology, USA, offers a comprehensive evaluation of color reproduction performance, surpassing the capabilities of the CRI. This metric proves invaluable in analyzing color quality, particularly in the context of solid-state lighting like LEDs. It accounts for factors such as hue preservation, chroma enhancement, gamut area index, and gamut shape index, providing an enhanced understanding of light source color performance and serving as a crucial tool for optimization. Upon increasing TiO$_2$ concentration, a noticeable decline is observed in both parameters. While the incorporation of BZG:Pr@TiO$_2$ enhances red emission intensity, higher quantities of TiO$_2$ particles do not invariably favor color reproduction, possibly due to scattering effects. The augmentation in blue-light utilization, facilitated by increased scattering efficiency through elevated TiO$_2$ content, benefits red-light generation for warm. However, due to diminished blue peak emission and reduced yellow-green emission intensity, the white light exhibits limitations in rendering a broad emission color spectrum, ultimately resulting in decreased CQS and CRI values. Thus, optimal TiO$_2$ particle concentration should remain low, and the incorporation of blue/green-emitting phosphors in conjunction with the proposed phosphor compound could yield enhanced color reproduction performance.

(a)   (b)
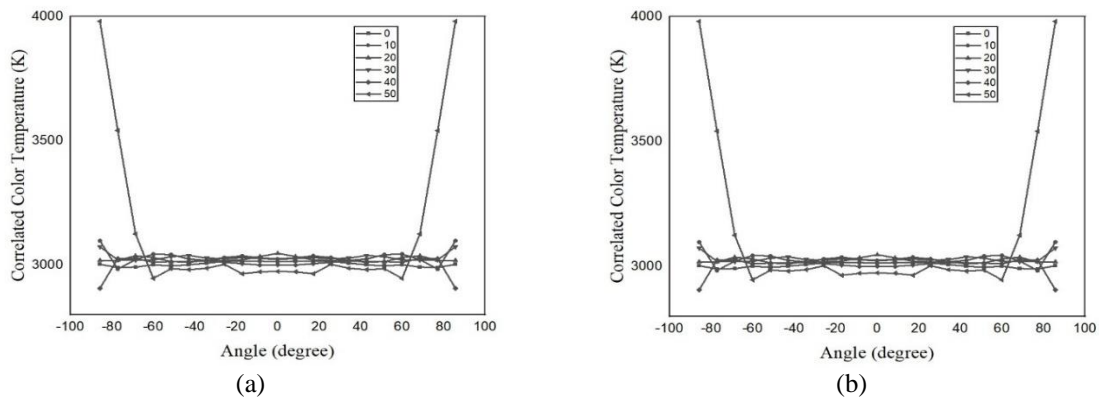
Figure 6. The chromatic uniformity when varying TiO$_2$ amount in BZG:Pr@TiO$_2$ compound
(a) angular CCT range and (b) deviated CCT level
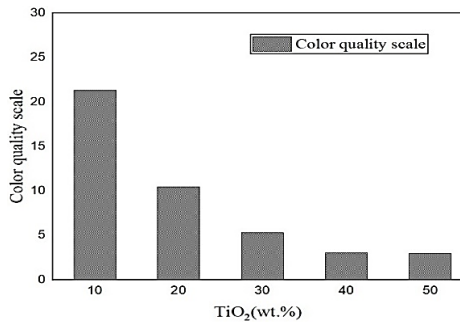
Figure 7. The CQS when varying TiO$_2$ amount in BZG:Pr@TiO$_2$ compound
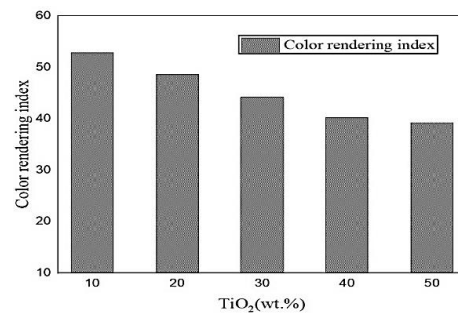
Figure 8. The CRI when varying TiO$_2$ amount in BZG:Pr@TiO$_2$ compound

4.   CONCLUSION

We investigated the impact of BZG:Pr@TiO$_2$ compound on the lighting characteristics of the LED package. The optical performance of the resulting LED was examined with different TiO$_2$ doping percentage from 10 wt% to 50 wt%. Findings reveal that the presence of the BZG:Pr@TiO$_2$ phosphor contributes to improved red spectrum performance, leading to enhanced color distribution uniformity. With the TiO$_2$ concentration lower than 50 wt%, the better color distributing uniformity is achievable, especially in the case of 20 wt% TiO$_2$ in the phosphor compound. However, an increase in TiO$_2$ content within the phosphor layer corresponds to a decrease in luminous power and chromatic reproduction efficiency of the LED, due to the redundant light scattering. Consequently, the light energy loss is significant as the scattered light is re-absorbed. Additionally, the blue light emission is diminished when the TiO$_2$ amount increases in red phosphor layer, leading to the lack of primary colors to access good lighting chromatic rendition. Optimal outcomes, in terms of luminosity and color quality, are achieved with a modest TiO$_2$ concentration of 10 wt%. Hence, it is advisable to maintain a lower TiO$_2$ particle concentration. The combination of blue/green-emitting phosphors and the suggested BZG:Pr@TiO$_2$ phosphor compound can result in a wide emission-color coverage, potential to enhance color reproduction performance of the LED model.

REFERENCES

[1]   M. Chlipala and T. Kozacki, "Color LED DMD holographic display with high resolution across large depth," *Optics Letters*, vol. 44, no. 17, pp. 4255–4258, 2019, doi: 10.1364/OL.44.004255.

[2]   K. J. Francis, Y. E. Boink, M. Dantuma, M. K. A. Singh, S. Manohar, and W. Steenbergen, "Tomographic imaging with an ultrasound and LED-based photoacoustic system," *Biomedical Optics Express*, vol. 11, no. 4, pp. 2152–2165, 2020, doi: 10.1364/BOE.384548.

[3]   S.-H. Lin *et al.*, "Enhanced external quantum efficiencies of AlGaN-based deep-UV LEDs using reflective passivation layer," *Optics Express*, vol. 29, no. 23, pp. 37835–37844, 2021, doi: 10.1364/OE.441389.

[4]   R. Yoshimura, D.-H. Choi, M. Fujimoto, A. Uji, F. Hiwatashi, and K. Ohbayashi, "Dynamic optical coherence tomography imaging of the lacrimal passage with an extrinsic contrast agent," *Biomedical Optics Express*, vol. 10, no. 3, pp. 1482–1495, 2019, doi: 10.1364/BOE.10.001482.

[5]   J. Li *et al.*, "On-chip integration of III-nitride flip-chip light-emitting diodes with photodetectors," *Journal of Lightwave Technology*, vol. 39, no. 8, pp. 2603–2608, 2021, doi: 10.1109/JLT.2020.3048986.

[6]   C.-M. Tsai, C.-S. Chang, Z. Xu, W.-P. Huang, W.-C. Lai, and J.-S. Bow, "Efficiency enhancement of III-nitride light-emitting diodes with strain-compensated thin-barrier InGaN/AlN/GaN multiple quantum wells," *OSA Continuum*, vol. 2, no. 4, pp. 1207–1214, 2019, doi: 10.1364/OSAC.2.001207.

[7]   M. Chlipala *et al.*, "Nitride light-emitting diodes for cryogenic temperatures," *Optics Express*, vol. 28, no. 20, pp. 30299–30308, 2020, doi: 10.1364/OE.403906.

[8]   A. Zhang *et al.*, "Enhanced amplified spontaneous emission from conjugated light-emitting polymer integrated with silicon nitride grating structures," *OSA Continuum*, vol. 2, no. 10, pp. 2875–2882, 2019, doi: 10.1364/OSAC.2.002875.

[9]   K. Tian *et al.*, "On the polarization self-screening effect in multiple quantum wells for nitride-based near ultraviolet light-emitting diodes," *Chinese Optics Letters*, vol. 17, no. 12, p. 122301, 2019, doi: 10.3788/COL201917.122301.

[10] A. Hassan, S. Khan, K. Rasul, and A. Hussain, "Lensless on-chip LED array microscope using amplitude and phase masks," *Journal of the Optical Society of America B*, vol. 37, no. 12, pp. 3652–3659, 2020, doi: 10.1364/JOSAB.396076.

[11] X. Gao *et al.*, "Circularly polarized light emission from a GaN micro-LED integrated with functional metasurfaces for 3D display," *Optics Letters*, vol. 46, no. 11, pp. 2666–2669, 2021, doi: 10.1364/OL.415150.

[12] S. Zhang *et al.*, "Efficient emission of InGaN-based light-emitting diodes: toward orange and red," *Photonics Research*, vol. 8, no. 11, pp. 1671–1675, 2020, doi: 10.1364/PRJ.402555.

[13] T. Zhang, X. Zhang, B. Ding, J. Shen, Y. Hu, and H. Gu, "Homo-epitaxial secondary growth of ZnO nanowire arrays for a UV-free warm white light-emitting diode application," *Applied Optics*, vol. 59, no. 8, pp. 2498–2504, 2020, doi: 10.1364/AO.385656.

[14] H. Goo, S. Mo, H. J. Park, M. Y. Lee, and J.-C. Ahn, "Treatment with LEDs at a wavelength of 642 nm enhances skin tumor proliferation in a mouse model," *Biomedical Optics Express*, vol. 12, no. 9, pp. 5583–5596, 2021, doi: 10.1364/BOE.427205.

[15] M. V. -Treviño, J. G. -Gutiérrez, J. M. R. -Lelis, and E. L. Apreza, "Optimizing an LED array for an infrared illumination source using the near field for venous pattern detection," *Applied Optics*, vol. 59, no. 9, pp. 2858–2865, 2020, doi: 10.1364/AO.381815.

[16] V.-C. Su and C.-C. Gao, "Remote GaN metalens applied to white light-emitting diodes," *Optics Express*, vol. 28, no. 26, pp. 38883–38891, 2020, doi: 10.1364/OE.411525.

[17] A. D. Griffiths *et al.*, "Multispectral time-of-flight imaging using light-emitting diodes," *Optics Express*, vol. 27, no. 24, pp. 35485–35498, 2019, doi: 10.1364/OE.27.035485.

[18] Z.-H. Xu, W. Chen, J. Penuelas, M. Padgett, and M.-J. Sun, "1000 fps computational ghost imaging using LED-based structured illumination," *Optics Express*, vol. 26, no. 3, pp. 2427–2434, 2018, doi: 10.1364/OE.26.002427.

[19] M. K. Hedili, B. Soner, E. Ulusoy, and H. Urey, "Light-efficient augmented reality display with steerable eyebox," *Optics Express*, vol. 27, no. 9, pp. 12572–12581, 2019, doi: 10.1364/OE.27.012572.

[20] E. M. A. Anas, H. K. Zhang, J. Kang, and E. Boctor, "Enabling fast and high quality LED photoacoustic imaging: a recurrent neural networks based approach," *Biomedical Optics Express*, vol. 9, no. 8, pp. 3852–3866, 2018, doi: 10.1364/BOE.9.003852.

[21] M. A. Khan, R. Takeda, Y. Yamada, N. Maeda, M. Jo, and H. Hirayama, "Beyond 53% internal quantum efficiency in a AlGaN quantum well at 326 nm UVA emission and single-peak operation of UVA LED," *Optics Letters*, vol. 45, no. 2, pp. 495–498, 2020, doi: 10.1364/OL.376894.

[22] H. Gu, M. Chen, Q. Wang, and Q. Tan, "Design of two-dimensional diffractive optical elements for beam shaping of multicolor light-emitting diodes," *Applied Optics*, vol. 57, no. 10, pp. 2653–2658, 2018, doi: 10.1364/AO.57.002653.

[23] E.-L. Hsiang, Q. Yang, Z. He, J. Zou, and S.-T. Wu, "Halo effect in high-dynamic-range mini-LED backlit LCDs," *Optics Express*, vol. 28, no. 24, pp. 36822–36837, 2020, doi: 10.1364/OE.413133.

[24] D. Chen *et al.*, "Improved electro-optical and photoelectric performance of GaN-based micro-LEDs with an atomic layer deposited AlN passivation layer," *Optics Express*, vol. 29, no. 22, pp. 36559–36566, 2021, doi: 10.1364/OE.439596.

[25] W. Wang and P. Zhu, "Red photoluminescent Eu^{3+}-doped Y$_2$O$_3$ nanospheres for LED-phosphor applications: synthesis and characterization," *Optics Express*, vol. 26, no. 26, pp. 34820–34829, 2018, doi: 10.1364/OE.26.034820.

[26] K. Chung, J. Sui, T. Sarwar, and P.-C. Ku, "Feasibility study of nanopillar LED array for color-tunable lighting and beyond," *Optics Express*, vol. 27, no. 26, pp. 38229–38235, 2019, doi: 10.1364/OE.382287.

BIOGRAPHIES OF AUTHORS

Le Thi Trang received a Master's degree in Information Technology from Lac Hong University, Vietnam, and is currently working as a lecturer at the Faculty of Information Technology, Dong Nai Technology University, Bien Hoa City, Vietnam. Her research interests include computer science, computer vision, image recognition and classification, face detection and recognition, abnormal motion detection, and graphic design. She can be contacted at email: lethitrang@dntu.edu.vn.

Le Xuan Thuy received the Master degree in physics from Can Tho University, Vietnam. She received a Ph.D. at Vietnam Academy of Science and Technology. She is working as a lecturer at the Faculty of Basic Sciences, Vinh Long University of Technology Education, Vietnam. Her research interests: as solar cells, OLED, photoanode, and theory physics. She can be contacted at email: thuylx@vlute.edu.vn.

Nguyen Le Thai received his BS in Electronic engineering from Danang University of Science and Technology, Vietnam, in 2003, MS in Electronic Engineering from Posts and Telecommunications Institute of Technology, Ho Chi Minh, Vietnam, in 2011 and Ph.D. degree of Mechatronics Engineering from Kunming University of Science and Technology, China, in 2016. He is a currently with the Nguyen Tat Thanh University, Ho Chi Minh City, Vietnam. His research interests include the renewable energy, optimisation techniques, robust adaptive control, and signal processing. He can be contacted at email: nlthai@ntt.edu.vn.

Thuc Minh Bui got his B.S. and M.S. degrees in Electrical Engineering from Ho Chi Minh City University of Technology and Education in 2005 and 2008, respectively, and his Ph.D. degree in electrical engineering at from Yeungnam University in Gyeongsan, Korea, in 2018. He is currently a lecturer at the Faculty of Electrical and Electronics Engineering at Nha Trang University in Nha Trang City, Vietnam. His scientific interests include control theory, power converter, automation, and optical science with applications to industry and the environment. He can be contacted at email: minhbt@ntu.edu.vn.